EXPLAINING AND FORECASTING INTERANNUAL VARIABILITY IN THE FLOW OF THE NILE RIVER

Mohamed S. Siam[1]

Ralph M. Parsons Laboratory, Massachusetts Institute of Technology, Cambridge, Massachusetts

Elfatih A. B. Eltahir

Ralph M. Parsons Laboratory, Massachusetts Institute of Technology, Cambridge, Massachusetts

[1]*Corresponding author address*: Mohamed Siam, Ralph M. Parsons Laboratory, Massachusetts Institute of Technology, 15 Vassar St. Cambridge, MA 02139.

E-mail:msiam@mit.edu

EXPLAINING AND FORECASTING INTERANNUAL VARIABILITY IN

THE FLOW OF THE NILE RIVER

Abstract

This study analyzes extensive data sets collected during the 20th century and define four modes of natural variability in the flow of Nile River, identifying a new significant potential for improving predictability of floods and droughts. Previous studies have identified a significant teleconnection between the Nile flow and the Eastern Pacific Ocean. El Niño-Southern Oscillation (ENSO) explains about 25% of the interannual variability in the Nile flow. Here, this study identifies a region in the southern Indian Ocean with similarly strong teleconnection to the Nile flow. Sea Surface Temperature (SST) in the region (50°E-80°E and 25°S-35°S) explains 28% of the interannual variability in the flow of Nile river and when combined with ENSO index the explained variability of the flow of Nile river increases to 44%. In addition, during those years with anomalous SST conditions in both Oceans, this study estimates that indices of the SSTs in the Pacific and Indian Oceans can collectively explain up to 84% of the interannual variability in the flow of Nile. Building on these findings, this study uses classical Bayesian theorem to develop a new hybrid forecasting algorithm that predicts the Nile flow based on global models predictions of indices of the SST in the Eastern Pacific and Southern Indian Oceans.

1. Introduction

The Nile basin covers an area of 2.9 $\times 10^6$ km^2, which is approximately 10% of the African continent (Fig. 1). It has two main tributaries; the White Nile and the Blue Nile that originate from the equatorial lakes and Ethiopian highlands respectively. The Upper Blue Nile (UBN) basin is the main source of water for the Nile River. It contributes to approximately 60% of the annual flow of the Nile and 80% of the total Nile flow that occurs between July and October at Dongola (Conway and Hulme, 1993) (Fig. 2). The UBN basin extends over an area of 175 $\times 10^3$ km^2 (7° N to $12^o5'$ N and from $34^o5'$ E to 40° E). The mean annual rainfall over this basin is 1200 mm/year (Conway and Hulme, 1993). Almost 60% of the annual rainfall over the UBN occurs during the summer between July and August, resulting in a largely predictable seasonal variability in the flow of the river.

The prediction of inter-annual variability in the flow of the Nile is rather challenging. Many studies investigated the teleconnections between the Ethiopian rainfall and the global Sea Surface Temperature (SSTs) in order to find SSTs indices to use for Nile flow prediction (e.g. Eltahir, 1996; Abtew et al., 2009; and Melesse et al., 2011). Eltahir (1996) showed that the SSTs anomalies over the tropical Eastern Pacific Ocean explains 25% of the inter-annual variability of Nile flow for the period 1872-1972. ElSanabary et al., 2014 showed that the dominant frequencies of the Ethiopian rainfall ranged between 2 and 8 years and that the scale averaged wavelet power of the SSTs over the Eastern Pacific and South Indian and Atlantic Oceans can explain significant fraction of the rainfall variability over Ethiopia using wavelet principal component analysis. These correlations between the Nile flow and SSTs indices were the basis for new forecast models that were proposed to predict the Nile flows. For example, Wang and Eltahir (1999) used a discriminant

45 prediction approach to estimate the probabilities that the Nile flow will fall into prescribed

46 categories. Eldaw et al., (2003) and Gissila et al., (2004) used sea surface temperature (SST) over

47 the Pacific, Indian and Atlantic Oceans as predictors within a multiple linear regression model to

48 predict the Nile flow.

49

50 The mechanisms behind these teleconnections between the rainfall over Ethiopia and the global

51 SSTs were examined in several studies (e.g. Beltrando and Camperlin, 1993). However, a clear

52 distinction must be made between rainfall over the UBN basin in Ethiopia and rainfall over East

53 Africa, defined as the region along the coast, east of the Ethiopian highlands (Fig. 1). The UBN

54 basin has one rainy season (May to September) during which more than 80% of the rainfall occurs,

55 while along the East coast of Africa and depending on the location from the equator, the seasonal

56 cycle of rainfall can have two rainy seasons (Black et al., 2003, Hastenrath et al., 2011). This

57 pattern in the seasonal cycle of rainfall is related to the migration of the Inter-tropical Convergence

58 Zone (ITCZ) across the equator. Camberlin, 1995 showed that the rainfall over East Africa,

59 including the UBN basin, is strongly coupled with the dynamics of the Indian monsoon. During

60 strong Indian monsoon seasons, the sea level pressure over India decreases significantly, which

61 enhances the pressure gradient between East Africa and India. As a result, westerly winds increase

62 over Eastern Africa and enhance transport moisture from the Congo basin to Ethiopia, Uganda and

63 western Kenya. Giro et al., 2010 also showed that the warming over the Pacific Ocean, during El

64 Niño events, reduces these westerly winds, which reduce the rainfall over East Africa. In addition,

65 the monsoon circulation is weaker during El Niño events due to modulation of the walker

66 circulation and enhanced subsidence over the Western Pacific and South Asia, thus the rainfall

67 over Ethiopia decreases (Ju and Slingo, 1995; Kawamura, 1998; Shukla and Wallace, 1983; Soman

68   and Slingo, 1997). The reduced Nile flows during El Niño events were also attributed to the

69   enhanced tropical-scale subsidence that suppresses rainfall, as a consequence of the increased

70   upwelling over the Eastern Pacific Ocean (Amarasekera et al., 1996).

71

72   The physical mechanism of the teleconnection between the Nile flow and SSTs of North and

73   Middle Indian Ocean and ENSO is described in another paper by the authors (Siam et al., 2014).

74   Nile flow is strongly modulated by ENSO through ocean currents. During El Niño events, the

75   warm water travels from the Pacific to the Indian Ocean through the "Indonesian through flow"

76   and advection by the Indian Equatorial Current (Tomczak and Godfrey, 1995). As a result, SSTs

77   in North and Middle Indian Ocean warm-up following the warming of Tropical Eastern Pacific,

78   and forces a Gill type circulation anomaly with enhanced westerly winds over Western Indian

79   Ocean (Yang et al., 2007). The latter enhances the low-level divergence of air and moisture away

80   from the Upper Blue Nile resulting in a reduction of rainfall over the basin. On the other hand, the

81   warming over the South Indian Ocean, generates a cyclonic flow in the boundary layer, which

82   reduces the cross-equatorial meridional transport of air and moisture towards the UBN basin,

83   favoring a reduction in rainfall and river flows. The tele-connections between the Pacific Ocean

84   and the Nile basin and between the Indian Ocean and the Nile basin are reflected in different modes

85   of observed natural variability in the flow of Nile River, with important implications for the

86   predictability of floods and droughts.

87

88   The objectives of the study are (i) to investigate the strength of the teleconnection between the

89   Indian Ocean and the Nile basin and its role in explaining observed natural modes of variability in

90   the flow of the Nile river, and (ii) to develop a new hybrid forecasting algorithm that can be used

91 to predict the Nile flow based on indices of the SST in the Eastern Pacific and Southern Indian

92 Oceans.

93

94 **2. Data**

95 In this study we use observed SSTs over the Indian and Pacific oceans from the monthly global

96 (HadISST V1.1) dataset on a 1 degree latitude-longitude grid from 1900 to 2000 (Rayner et al.

97 2003). The monthly flows at Dongola from 1900 to 1984 were extracted from the Global River

98 Discharge Database (RivDIS v1.1) (Vörösmarty et al., 1998) and from 1984 to 2000 through

99 personal connection. The average monthly anomalies from September to November of the SSTs

100 averaged over the Eastern Pacific Ocean (6ºN-2ºN, 170ºW-90ºW; 2ºN-6ºS, 180ºW-90ºW; and

101 6ºS-10ºS, 150ºW-110ºW) are used as an index of ENSO. This area has shown the highest

102 correlation with the Nile flows and it is almost covering the same area as Niño 3 and 3.4 indices

103 (Trenberth, 1997).

104

105 **3. Relation between the variability in the flow of Nile river, ENSO and the Indian Ocean SST**

106 Based on extensive correlation analysis of the Nile river flow at Dongola and the observed SST in

107 the Indian Ocean, this study identifies a region over the Southern Indian Ocean (50ºE-80ºE and

108 25ºS-35ºS) (see Figure 3) as the one with the highest correlation between SST and the Nile flow.

109 This correlation is especially high for river flow (accumulated for July, August, September and

110 October) and SST during the month of August. An earlier study by ElDaw et al. (2003) used SST

111 indices over the Indian Ocean to predict the Nile flow, however, they focused on regions of the

112   Indian Ocean that are different from the region that we use in defining the South Indian Ocean

113   (SIO) index. In other words the region of the SIO was not used by ElDaw et al. (2003). Table 2

114   describes the regions of the Indian Ocean identified in both studies.

115
116   This study emphasizes that the proposed forecasting methodology for the Nile flow is motivated

117   by the physical mechanisms proposed by Siam et al. (2014) and described in Section 1. In contrast,

118   the forecasting approach of some of the previous studies was based on purely statistical

119   correlations found between the Nile flow and SSTs globally.

120

121   Figure 4 shows the observed and simulated time series of the average July to October Nile flow at

122   Dongola, which accounts for approximately 70% of the annual Nile flow. The Nile flow is

123   predicted by three different linear regression models using either ENSO averaged from September

124   to November (Figure 4a) or SIO August (Figure 4b) indices, or both (Figure 4c) as covariates. It

125   is clear from this figure that the addition of the SIO index increase the explained variability of the

126   Nile flow to 44%, compared to only 30% when ENSO index is used alone. This indicates that the

127   SIO index can explain almost 14% of the variability of the Nile flow that is independent from

128   ENSO. The North and middle of the Indian Ocean have also exhibited a high correlation between

129   their SST and the Nile flow. However, the additional variability explained by the SST over the

130   North and Middle Indian Ocean, when combined with the ENSO index, is negligible (not shown

131   here). This is mainly because the SSTs over the North and Middle Indian Ocean are dependent on

132   ENSO, while the SSTs over the South Indian Ocean (i.e. SIO index) is not, as described in Section

133   1.

134

135 In further analysis, we define ±0.5°C as the threshold between non-neutral and neutral years on the

136 Eastern Pacific Ocean based on ENSO index. This value is about two-thirds of one standard

137 deviation of the anomalies of ENSO index. The same threshold has been used to identify non-

138 neutral and neutral years using El Niño 3.4 index, which is similar to our ENSO index (Trenberth,

139 1997). This indicates that if the ENSO index anomaly is greater than 0.5°C or less than -0.5°C, it

140 is considered as non-neutral condition, otherwise, it is considered as neutral condition. Similarly,

141 ±0.3°C value is used as a threshold between non-neutral and neutral years on the South Indian

142 Ocean using the SIO index. This value is also about two-thirds of one standard deviation for the

143 anomalies of the SSTs over this region. Thus, if both ENSO and SIO indices are used together,

144 four different combinations can be defined based on these classifications. The first is when both

145 ENSO and SIO indices are neutral (29 out of 100 events), the second is when both ENSO and SIO

146 indices are non-neutral (19 out of 100 events), the third when SIO is non-neutral and ENSO is

147 neutral (26 out of 100 events) and finally when SIO is neutral and ENSO is non-neutral (26 out of

148 100 events). Each of these combinations is considerate as a mode of natural variability in the flow

149 of Nile river. Then the Nile flow is calculated as a predictant using multiple linear regression with

150 the (ENSO and SIO indices) of each mode as predictors.

151

152 Four different modes are identified for describing the natural variability in the flow of Nile River

153 and summarized in (Table 1). The ENSO and SIO indices do not explain a significant fraction of

154 the interannual variability in the flow of river when they are both neutral (Fig. 5a). The variability

155 of the Nile flow in such years can be regarded as a reflection of the chaotic interactions between

156 the biosphere and atmosphere and within each of the two domains. For this mode, the predictability

157 of the Nile flow is rather limited. The other two intermediate modes include non-neutral conditions

158   in the Eastern Pacific and neutral conditions in the Southern Indian Oceans or vice versa (Fig. 5b

159   and 5c). For these two modes, a significant fraction (i.e. 31% and 43%) of the variance describing

160   inter-annual variability in the flow is explained. Hence, these modes point to a significant potential

161   for predictability of the flow. Finally, indices of ENSO and SIO can explain 84% of the interannual

162   variability in the Nile flow when non-neutral conditions are observed for both the Eastern Pacific

163   and Southern Indian Oceans (Fig. 5d). Therefore, the SIO index can be used to predict the flow

164   together with the ENSO index, as collectively they can explain a significant fraction of the

165   variability in the flow of Nile River. This result indicates that during years with anomalous SST

166   conditions in both oceans, floods and droughts in the Nile River flow can be highly predictable,

167   assuming accurate forecasts of those indices are available.

168

4. A Hybrid Methodology for Long-range Prediction of the Nile flow

169

170   A simple methodology is proposed to predict the Nile flow with a lead time of about a few months

171   (~3-6 months). The forecast of global SST distribution based on dynamical models (e.g. NCEP

172   coupled forecast system model version 2 (CFSv2), Saha et al., 2010; Saha et al., under review),

173   can be used together with the algorithm developed in this section to relate the Nile flow to ENSO

174   and SIO indices. The proposed method is shown in Figure 6 and can be described in two main

175   steps:

176   •   Forecast of SST anomalies in the Indian Ocean and Eastern Pacific Ocean using dynamical

177   models of the coupled global ocean atmosphere system. Such forecasts are routinely issued by

178   centers such NCEP and ECMWF.

179   •   Application of a forecast algorithm between the Nile flow (predictand) and forecasted SSTs

180   in the Indian and Eastern Pacific Oceans (predictors) for the identified mode of variability.

181

182   In this paper we focus on the second step of the proposed method: the development of the algorithm

183   relating SSTs and the Nile flow. We develop the forecast algorithm using observed SSTs. We do

184   not describe how this algorithm can be applied with forecasts of global SST distribution based on

185   dynamical models as this step is beyond the scope of this paper. However, we recognize that

186   overall accuracy of this method in predicting interannual variability of the Nile flow is dependent

187   on the skill of global coupled models in forecasting the global SSTs (See Appendix for information

188   about forecasting models). Thus, the selection of the forecast model, which predicts the SSTs is

189   an important step to ensure the accuracy of the prediction of the Nile flow. As global coupled

190   ocean-atmosphere models improve in their skill of forecasting global SSTs in the Pacific and

191   Indian Oceans, we expect that our ability to predict the interannual variability in the Nile flow will

192   improve too. In addition, the accuracy in the prediction of the Nile flow at medium and short time

193   scales (of weeks to one month) can be improved by adding other hydrological variables (e.g.

194   rainfall and stream flow) over the basin, as demonstrated by (Wang and Eltahir, 1999)

195   The proposed method can be described as hybrid since it combines dynamical forecasts of global

196   SSTs, and statistical algorithms relating the Nile flow and the forecasted SSTs. The same method

197   can also be described as hybrid since it combines information about SSTs from the Pacific and the

198   Indian Oceans.

199   Here, we apply a discriminant approach that specifies the categoric probabilities of the predictand

200   (Nile flow) according to the categories that the predictors (i.e. ENSO and SIO indices) fall into.

201   The annual Nile flow is divided into "low", "normal", and "high" categories. The boundaries of

202   these categories are defined so that the number of points in each category is about a third of the

203   data points (Fig 7). On the other hand, the ENSO and SIO indices are divided into "cold", "normal"

204   and "warm" categories. (The words Normal and Neutral are used to describe the same

205   conditions).The boundaries for the normal category are -0.5°C and 0.5°C for ENSO index and -

206   0.3°C and 0.3°C for SIO index (Fig. 7). Any condition below the lower limit is considered "cold"

207   and higher than the upper limit is considered "warm" for both indices.

208   The Bayesian theorem, described in many statistical books (e.g., Winkler 1972; West 1989), states

209   that the probability of occurrence of a specified flow category (Q_i) and given two conditions (A

210   and B) can be expressed as

211

$$P(Q_i/\,A,B) \; = \frac{P(B/Q_i,A)P(Q_i/A)}{P(B/A)} \qquad (1)$$

212   Where $P(Q_i/\,A)$ is the probability of event Q_i given that event A has occurred, and $P(Q_i/\,A,B)$ is

213   the probability of event Q_i given that events A and B have occurred, and similarly for other shown

214   probabilities. In addition, if the events A and B are independent, we can rewrite Eq. (1) as

215

$$P(Q_i/\,A,B) \; = \frac{P(B/Q_i)P(Q_i/A)}{\sum_{i=1}^{3} P(B/Q_i)P(Q_i/A)} \qquad (2)$$

216   The advantage of assuming independence between (A and B) and using Eq. (2), it simplifies the

217   calculation of P(B/Q$_i$, A) since we do not have to split the data into a relatively large number of

218   categories, which reduces the error due to the limitation of the data size. The independence

219   between ENSO and SIO indices is a reasonable assumption as the coefficient of determination

220   between them is less than 6%.

221

222   In order to evaluate the predictions of the Nile flow, we use a forecasting index (FI) defined by

223   Wang and Eltahir, (1999) as

224 $$FP(j)= \sum_{i=1}^{3} P_r(i,j)\, P_p(i,j) \quad (3)$$

225 $$FI = \frac{1}{n}\sum_{i=1}^{n} FP\,(j) \quad\quad\quad (4)$$

226   Where FP(j) is the forecast probability in a certain year (j) and the FI is the average of the FP over

227   a certain period, n. The prior probability $P_r(i, j)$ is calculated using Eq.(2) for a certain year (j) and

228   category (i=1, 2, 3) and the posterior probability $P_p(i, j)$ is defined as [1,0,0] in low flow year,

229   [0,1,0] in normal year, and [0,0,1] in a high flow year. Hence, a larger FI indicates a higher

230   accuracy of the forecast. The FI without any information about SST, should be about one third as

231   we have classified flow data into three categories each with a similar number of the data points.

232   The data is split into a calibration period (1900-1970) and a verification period (1970-2000).

233   Tables 3 and 4 summarize the conditional probabilities of Nile flow given certain conditions of

234   SIO or ENSO index. It is shown that during "warm" and "cold" conditions of SIO, the probabilities

235   are significantly higher for "low" and "high" Nile flow, respectively. The same is true for the

236   ENSO, as was described originally by Eltahir (1996). Table 5 shows the probabilities that are

237   conditioned on both SIO and ENSO, calculated using Eq. (2). This table illustrates clearly how

238   forecasts of the Nile flow can be improved by combining the two indices. For example, "warm"

239   conditions in both oceans translate into 85% probability of "low" flow in the Nile, and insignificant

240   probability of "high" flow. On the other hand, "cold" conditions in both oceans translate into 83%

241   probability of "high" flow in the Nile, and insignificant probability of "low" flow. Depending on

242   the accuracy of the dynamical forecast models of global SSTs, such forecast of the Nile flow can

243   be issued with lead times of 6 months. At present, the Eastern Nile Regional technical Office

244 (ENTRO) issues operational forecasts of the Nile flow based on ENSO forecasts and the

245 probability table described by Eltahir (1996) (similar to Table 4). We anticipate that use of Table

246 5, would represent a significant improvement in these operational forecasts.

247 The combined use of ENSO and the SIO indices significantly increased the FI to 0.5 (Figure 8a).

248 Comparison of Figures 8b and 8c, illustrates that the SIO index alone has almost the same FI value

249 as ENSO index. Recall that in absence of any information about global SSTs, the FI should have

250 a value of one third. The deviations of the FI using ENSO index alone (Figure 8b) or SIO index

251 alone (Figure 8c) from one third are almost added together to create the deviation of the FI from

252 the hybrid method from one third (Figure 8a). Hence, the new SIO index plays an independent role

253 from ENSO in shaping the interannual variability in the flow of Nile River. Thus by using these

254 two indices, we explain a significant fraction of the interannual variability in the flow of Nile

255 River, and illustrate a significant potential for improving the Nile flow forecasts.

5. Conclusions

257 • In this paper, we document that the SSTs in the Eastern Pacific and Indian Oceans play a

258 significant role in shaping the natural interannual variability in the flow of Nile River.

259 Previous studies have identified a significant teleconnection between the Nile flow and the

260 Eastern Pacific Ocean. El Niño-Southern Oscillation (ENSO) explains about 25% of the

261 interannual variability in the Nile flow. Here, this study identifies a region in the southern

262 Indian Ocean with similarly strong teleconnection to the Nile flow. Sea Surface

263 Temperature (SST) in the region (50°E-80°E and 25°S-35°S) explains 28% of the

264 interannual variability in the Nile flow.

265 • In addition, four different modes of natural variability in the Nile flow are identified and it

266 is shown that during non-neutral conditions in both the Pacific and Indian Oceans, the Nile

267   flow is highly predictable using global SST information. During those years with

268   anomalous SST conditions in both Oceans, this study estimates that indices of the SSTs in

269   the Pacific and Indian Oceans can collectively explain up to 84% of the interannual

270   variability in the flow of Nile. The estimated relationships between the Nile flow and these

271   indices allow for accurately predicting the Nile floods and droughts using observed or

272   forecasted conditions of the SSTs in the two oceans.

273   •   This study uses classical Bayesian theorem to develop a new hybrid forecasting algorithm

274   that predicts the Nile flow based on indices of the SST in the Eastern Pacific and Southern

275   Indian Oceans. "Warm" conditions in both oceans translate into 85% probability of "low"

276   flow in the Nile, and insignificant probability of "high" flow. On the other hand, "cold"

277   conditions in both oceans translate into 83% probability of "high" flow in the Nile, and

278   insignificant probability of "low" flow. Applications of the proposed hybrid forecast

279   method should improve predictions of the interannual variability in the Nile flow, adding

280   a new a tool for better management of the water resources of the Nile basin.

281   The proposed forecasting methodology is indeed dependent on the accuracy of the global SST

282   forecasts from global dynamical models. The accuracy of these forecasts is likely to improve as

283   the models are tested and developed further. However, in this paper we test the proposed

284   forecasting algorithm using observed SSTs. Such test describes an upper limit of the skill of the

285   proposed algorithm. The assessment of the same methodology using indices of SST forecasted by

286   global dynamical models will be addressed in future work.

287

288

Tables

Table 1: Summary of the coefficient of determination (R^2) between the average Nile flow from July to October and different combination of indices of ENSO and SIO.

Mode		ENSO	SIO	ENSO, SIO	Number of events (Observed Variance of Nile flow)
ENSO	SIO				
Neutral	Neutral	0.04	0.03	0.08	29 (6.76)
Neutral	Non-Neutral	0.05	0.28[+]	0.31[+]	26 (10.24)
Non-Neutral	Neutral	0.4[+]	0.02	0.43[+]	26 (5.8)
Non-Neutral	Non-Neutral	0.64[+]	0.6[+]	0.84[+]	19 (12.3)

Note: The values between brackets are for the observed variance of Nile flow of each mode in units of (MCM^2/day^2)

SIO: South Indian Ocean SSTs index, ENSO: ENSO index.

*Values that are significant at 5% significance level

[+] Values that are significant at 1% significance level

302

Table 2: Comparison between regions in the Indian Ocean used in ElDaw et al., 2003 and this study to predict the Nile flow.

Region	Location	Study
1	(35º-44 º S, 115 º -130 º E)	ElDaw et al, 2003
2	(0º-7 º S, 90 º -130 º E)	
3	(35º-44 º S, 20 º -60 º E)	
4	(10º-20 º S, 110 º -125 º E)	
5	(50ºE-80ºE and 25ºS-35ºS)	This study

305

Table 3: Conditional probability of the Nile flow given SIO conditions

		Nile flow		
		High	Normal	Low
SIO	Warm	0	0.25	0.75
	Normal	0.23	0.39	0.39
	Cold	0.57	0.26	0.17

307

308

309

310

311

312   **Table 4:** Conditional probability of the Nile flow given ENSO conditions

		Nile flow		
		High	Normal	Low
ENSO	Warm	0.15	0.31	0.54
	Normal	0.22	0.38	0.41
	Cold	0.68	0.32	0

313

314

315   **Table 5:** Conditional probability of the Nile flow given SIO and ENSO conditions

SIO	Nile flow	ENSO		
		Warm	Normal	Cold
SIO Warm	High	0	0	0
	Normal	0.15	0.22	1
	Low	0.85	0.78	0
SIO Normal	High	0.1	0.14	0.57
	Normal	0.31	0.4	0.43
	Low	0.59	0.46	0
SIO Cold	High	0.33	0.42	0.83
	Normal	0.29	0.33	0.17
	Low	0.37	0.25	0

316

317

318

Appendix

320 **Table 1:** Summary of some available forecast models of the Sea Surface Temperature

Model	Type of Model	Agency	Domain	Lead time up to (Months)	Resolution (km)	Reference
NCEP-CFS V2	Dynamical	National Centers for Environmental Prediction (NCEP)	Global	8	200	Saha et al., 2010
NASA-GMAO	Dynamical	NASA Goddard Space Flight Center- Global Modeling and Assimilation Office	Global	12	200	Bacmeister et al., 2000
ECMWF-System 4	Dynamical	European Centre for Medium-Range Weather Forecasts	Global	4	70	Molteni et al., 2011
UKMO-GCM	Dynamical	United Kingdom Met Office	Global	6	150	Graham et al., 2005
NOAA-CDC	Statistical	National Oceanic and Atmospheric Administration-Climate Diagnostic Center	Global	12	--	Pneland et al., 1998
CPC-Markov	Statistical	National Centers for Environmental Prediction-Climate Prediction Center	Nino 3 and Nino 3.4	8	--	Xue et al., 2000

321

REFRENCES

1. Abtew, W., Melesse, A. M. and Dessalegne, T. (2009), El Niño Southern Oscillation link to the Blue Nile River Basin hydrology. Hydrol. Process., 23: 3653–3660. doi: 10.1002/hyp.7367

2. Amarasekera, K. N., Lee, R. F., Williams, E. R., and Eltahir, E. A. B: ENSO and the natural variability in the flow of tropical rivers, J. Hydrol., 200, 24–39, 1996.

3. Beltrando, G., and Camberlin, P., 1993: Interannual variability of rainfall in Eastern Horn of Africa and indicators of atmospheric circulation. International Journal of climatology 13, 533-546.

4. Bacmeister, J. T., P. J. Pegion, S. D. Schubert, and M. J. Suarez, 2000: Atlas of seasonal means simulated by the NSIPP1 atmospheric GCM, NASA Tech. Memo-2000-104606, Vol. 17, 194pp.

5. Black E., J. Slingo, and K.R. Sperber, 2003: An observational study of the relationship between excessively strong short rains in coastal East Africa and Indian Ocean SST. Mon. Wea. Rev., 31, 74-94.

6. Camberlin P., 1995. June-September rainfall in North-Eastern Africa and atmospheric signals over the tropics: a zonal perspective. International Journal of Climatology 15: 773-783.

7. Camberlin, Pierre, 1997: Rainfall Anomalies in the Source Region of the Nile and Their Connection with the Indian Summer Monsoon. J. Climate, 10, 1380–1392.

8. Conway, D., and M. Hulme, 1993: Recent Fluctuations in precipitation and runoff over the Nile subbasins and their impact on Main Nile discharge. Climatic Change, 25, 127 -151.

9. ElDaw, A., J. D. Salas, and L. A. Garcia, 2003: Long Range Forecasting of the Nile River Flows Using Climate Forcing. J. Applied Meteorology, 42:890-904.

10. Eltahir, E. A. B., 1996: ElNino and the natural variability in the flow of the Nile river. Water Resour. Res., 32(1): 131-137.

11. Hastenrath, Stefan, Dierk Polzin, and Charles Mutai, 2011: Circulation Mechanisms of Kenya Rainfall Anomalies. J. Climate, 24, 404–412.

12. Ju, J., and J. M. Slingo, 1995: The Asian summer monsoon and ENSO.Quart. J. Roy. Meteor. Soc., 121, 1133–1168.

364   13. Kawamura, R., 1998: A possible mechanism of the Asian summer monsoon-ENSO
365   coupling. J. Meteor. Soc. Japan, 76, 1009–1027.

366

367   14. Melesse, A., Abtew, W. Setegn, S.G., Desalegn, T. (2011). Hydrological Variability
368   and Climate of the Upper Blue Nile River Basin. In Nile River Basin: Hydrology,
369   Climate and Water Use. Springer. Melesse, Assefa M. (Ed.), 1st Edition., 2011, X,
370   480 p. 200 illus, Part 1, 3-37, DOI: 10.1007/978-94-007-0689-7_1

371

372   15. Molteni, F., T. Stockdale, M. Balmaseda, G. Balsamo, R. Buizza, L. Ferranti, L.
373   Magnusson, K. Mogensen, T. Palmer & F. Vitart, 2011: The new ECMWF seasonal
374   forecast   system   (System   4).   ECMWF   Research   Department   Technical
375   Memorandum n.656, ECMWF, Shinfield Park, Reading RG2-9AX, UK, pp. 51.

376
377   16. ElSanabary, M. H., Gan, T. Y., Mwale, D., 204: Application of wavelet empirical
378   orthogonal function analysis to investigate the nonstationary character of Ethiopian
379   rainfall and its teleconnection to nonstationary global Sea Surface Temperature
380   variations   for   1900-1998.   International   Journal   of   Climatology.
381   DOI:10.1002/joc.3802

382

383   17. Graham. R., M. Gordon, P.J. McLean, S. Ineson, M.R. Huddleston, M.K. Davey, A.
384   Brookshaw, R.T.H. Barnes, 2005: A performance comparison of coupled and
385   uncoupled versions of the Met Office seasonal prediction general circulation
386   model. Tellus, 57A, 320-339.

387

388   18. Giro, D. Grimes, D., Black, E. 2011: Teleconnections between Ethiopian summer

389   rainfll and sea surface temperature: part I Observation and Modeling. Climate

390   Dynamics 37:103-199.

391

392   19. Gissila, T., Black, E., Grimes, D. I. F., Slingo, J.M 2004: Seasonal forecasting of the

393   Ethiopian Summer rains. International Journal of Climatology 24: 1345-1358.

394

395   20. Penland, C. and L. Matrosova, 1998: Prediction of Tropical Atlantic Sea Surface

396   Temperatures Using Linear Inverse Modeling. J. Climate, 11, 483-496.

397

398   21. Saha, Suranjana, and Coauthors, 2010: The NCEP Climate Forecast System

399   Reanalysis. Bull. Amer. Meteor. Soc., 91, 1015.1057. doi:

400   10.1175/2010BAMS3001.1.

401

402   22. Suranjana Saha, Shrinivas Moorthi, Xingren Wu, Jiande Wang, Sudhir Nadiga,

403   Patrick Tripp, Hua-Lu Pan, David Behringer, Yu-Tai Hou, Hui-ya Chuang, Mark

404   Iredell, Michael Ek, Jesse Meng, Rongqian Yang, Huug van den Dool, Qin Zhang,

405   Wanqiu Wang, Mingyue Chen, 2013 : The NCEP Climate Forecast System

406   Version 2. (Journal of Climate, under review.)

407

408   23. Shukla, J., and J. M. Wallace, 1983: Numerical simulation of the atmospheric

409   response to equatorial Pacific sea surface temperature anomalies. J. Atmos. Sci., 40,

410   1613–1630.

411

24. Siam, M. S., Wang, G., Estelle, ME., and Eltahir, E. A. B, 2014: Role of the Indian
    Ocean Sea Surface Temperature in shaping natural variability in the flow of the Nile
    River. Climate Dynamics, in press.

415

25. Soman, M. K., and J. Slingo, 1997: Sensitivity of the Asian summer monsoon to
    aspects of sea-surface-temperature anomalies in the tropical pacific ocean. Q. J. R.
    Meteorol. Soc., 123, 309-336.

419

26. Trenberth, K. E., 1997: The Definition of El Niño. Bulletin of the American
    Meteorological Society, 78, 2771-2777.

422

27. Wang, G., and Eltahir E. A. B, 1999: Use of ENSO information in Medium and
    Long Range Forecasting of the Nile Floods . J. Climate, 12, 1726-1737.

28. West, M., 1989: Bayesian Forecasting and Dynamic Models. Springer, 704 pp.

426

427
29. Winkler, R., 1972: An introduction to Bayesian inference and Decision. Holt,
    Rinchart and Winstoon, 563 pp.

430

30. Xue, Y., A. Leetmaa, and M. Ji, 2000: ENSO prediction with Markov model: The
    impact of sea level. J. Climate, 13, 849-871.

433

434   31. Yang, J. L., Q. Y. Liu, S. P. Xie, et al., 2007: Impact of the Indian Ocean SST basin

435   mode on the Asian summer monsoon, Geophys. Res. Lett., 34, L02708,

436   doi:10.1029/2006GL028571.

437

438

439

440

441

442
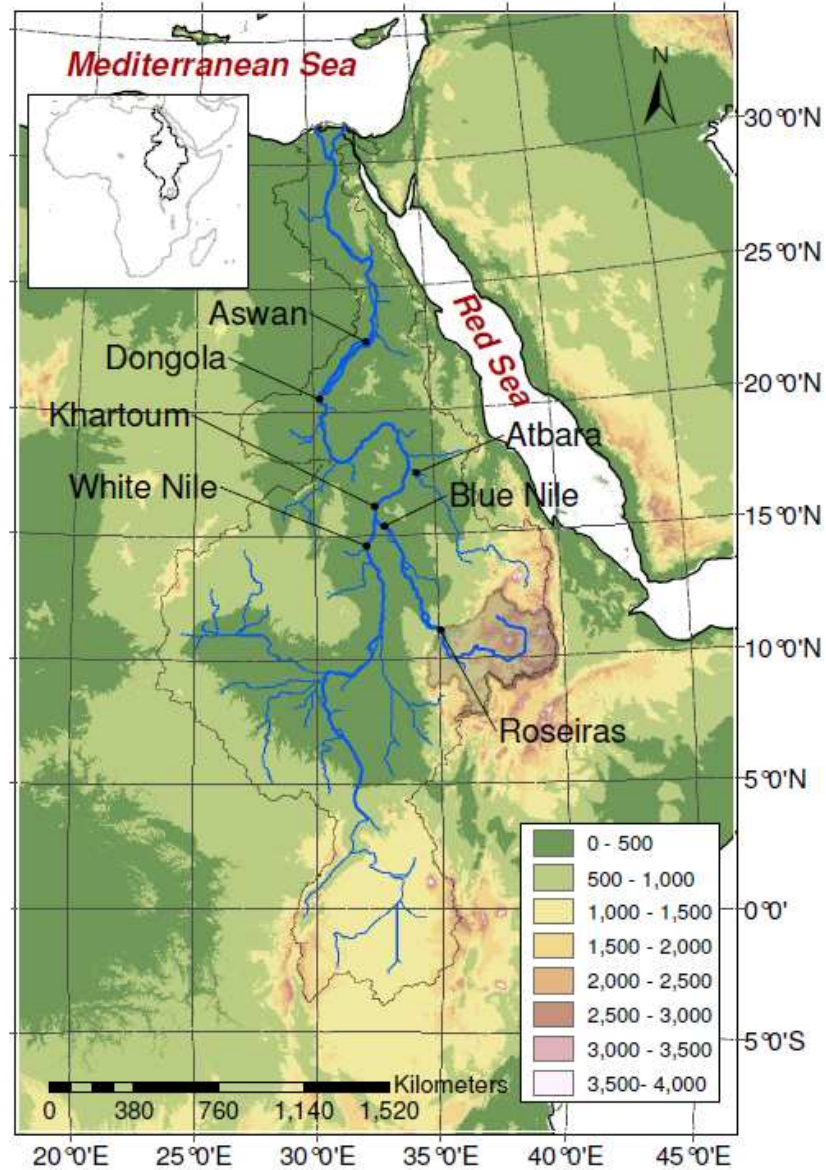
443

444

445
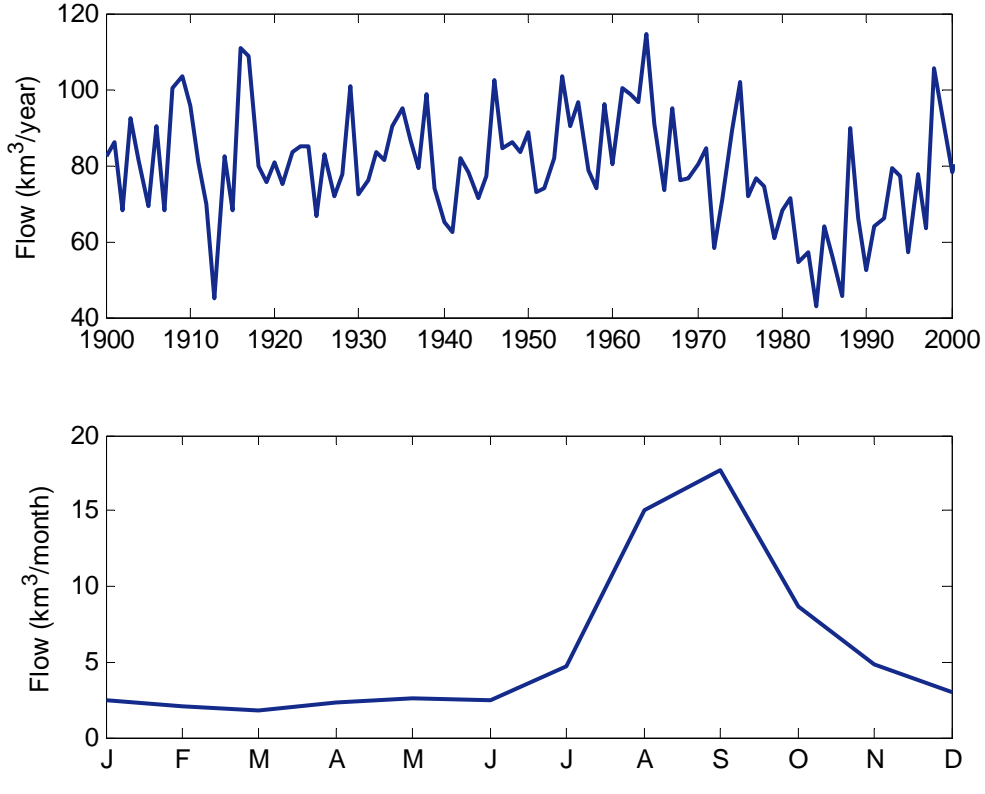
446

447

448

449

450

451

452

453

454

455

456

Figures

Figure 1: Topographic map of the Nile basin showing the outlet of the Upper Blue Nile basin (shaded in gray) at Roseiras. The White and Blue Nile join together at Khartoum the form the main branch of the Nile that flows directly to Dongola in the North.

465

466

480 **Figure 2:** Annual Nile flow (Top) and seasonal cycle (Bottom) of the flow at Dongola for the period from
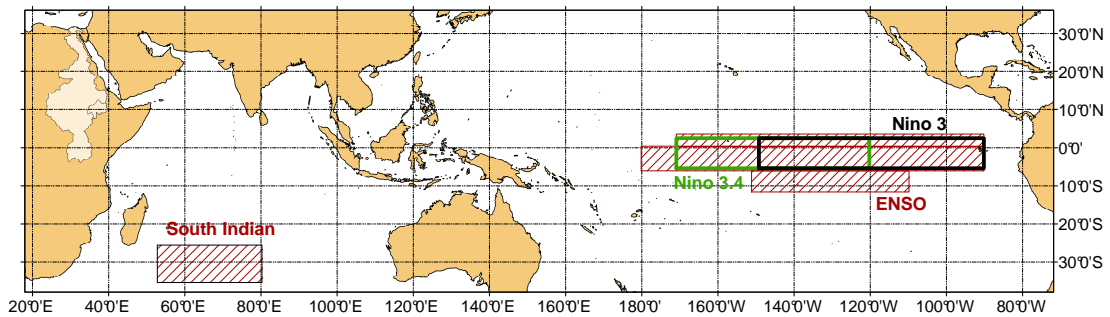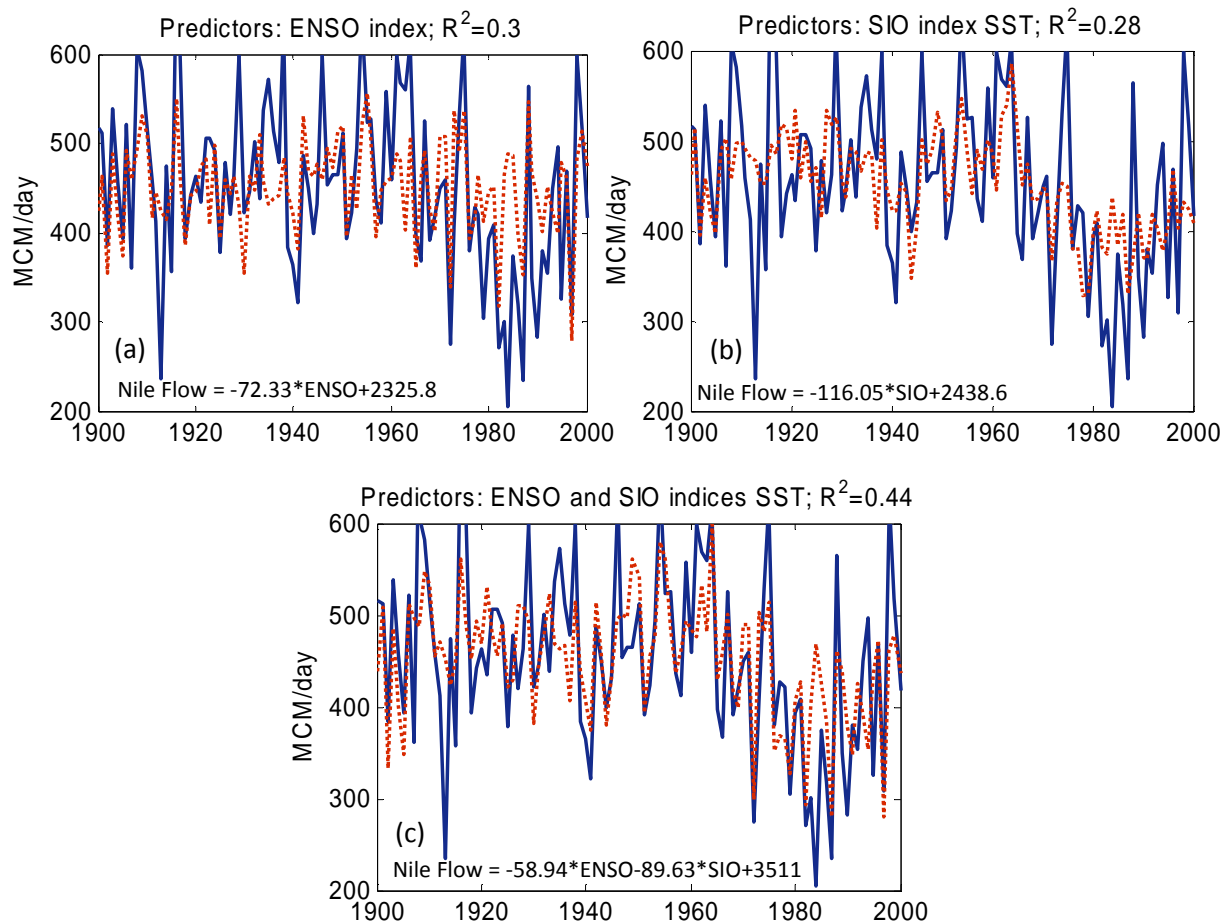481 1900 to 2000.

482

483

489 **Figure 3:** World map showing areas that cover the ENSO and North and South Indian Ocean SSTs indices.
490 The Nino 3 and 3.4 are outlined in black and green respectively. The whole Nile basin is outlined in black.

491

Figure 4: Observed (Solid Blue lines) and simulated (Dashed Red lines) average Nile flows in Million Cubic Meter per day (MCM/day) from July to October at Dongola using: a) ENSO index, b) SIO index and c) ENSO and SIO indices as predictors for the period 1900 to 2000. The simulated flows are calculated based on the equations shown in each figure, in which the predictands are the average observed SSTs over the ENSO and SIO regions in degrees Celsius and the predictor is the average Nile flow from July to October in Million Cubic Meter per day (MCM/day).

492

493
494
495
496
497
498

499

500

501

502
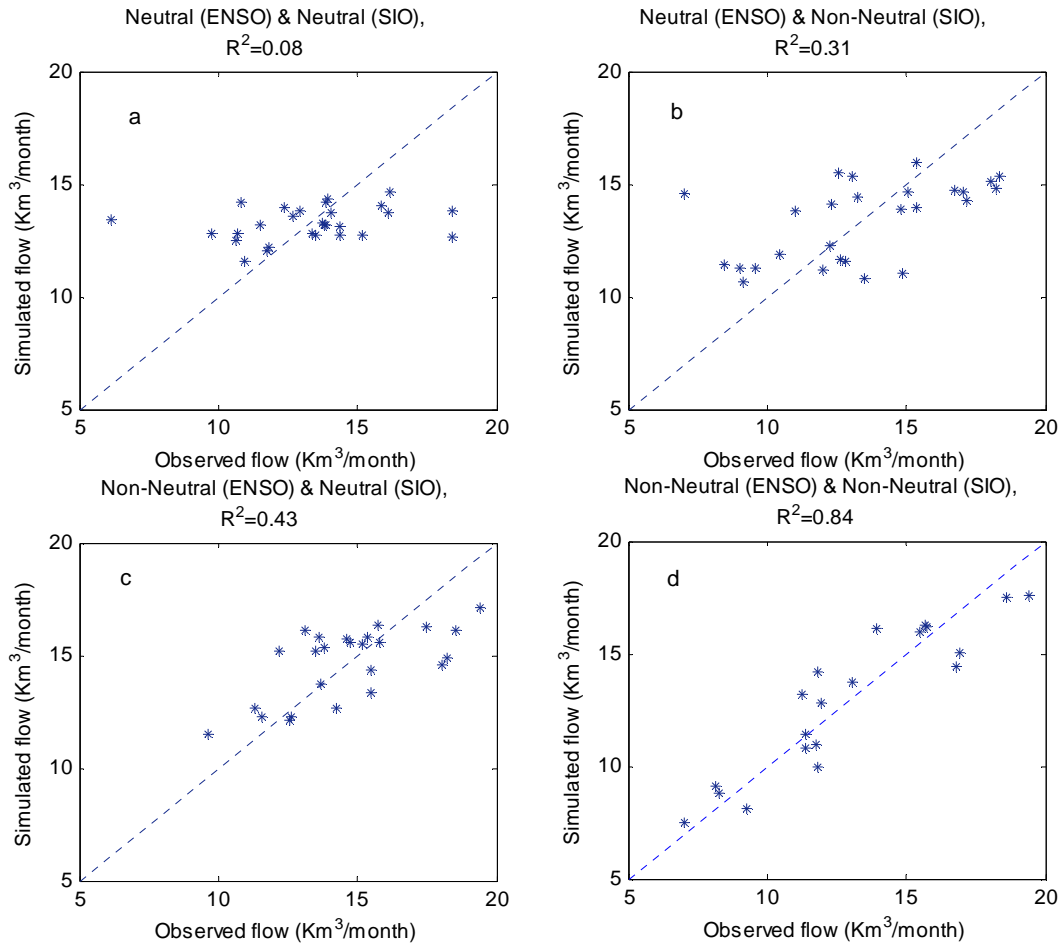
Figure 5: A comparison between the observed and simulated Nile flow showing the different modes of variability for the period from 1900 to 2000: a) Neutral ENSO (29 events) and SIO, b) Neutral ENSO and Non-Neutral SSTs in SIO (26 events), c) Non-Neutral ENSO and Neutral SSTs in SIO (26 events) and finally, d) Non-Neutral ENSO and Non-Neutral SSTs in SIO (19 events).
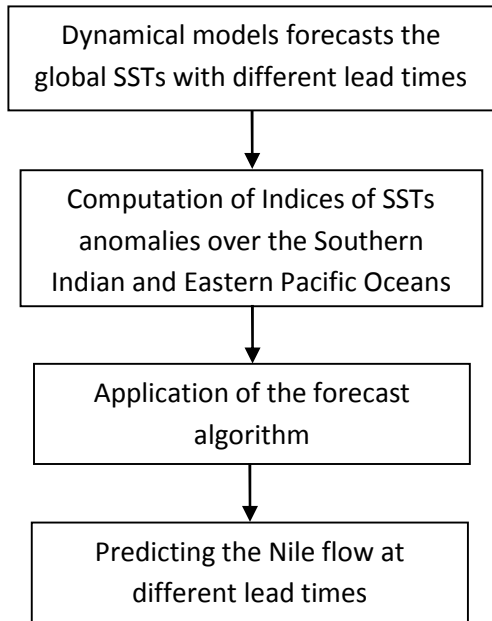
516

517

518

519

520

521

522

523

524

525

526

```
┌─────────────────────────────────┐
│   Dynamical models forecasts the │
│  global SSTs with different lead times │
└─────────────────────────────────┘
                 │
                 ▼
┌─────────────────────────────────┐
│   Computation of Indices of SSTs │
│      anomalies over the Southern │
│  Indian and Eastern Pacific Oceans │
└─────────────────────────────────┘
                 │
                 ▼
┌─────────────────────────────────┐
│     Application of the forecast  │
│            algorithm             │
└─────────────────────────────────┘
                 │
                 ▼
┌─────────────────────────────────┐
│     Predicting the Nile flow at  │
│         different lead times     │
└─────────────────────────────────┘
```

Figure 6: Schematic of the hybrid methodology for predicting the Nile flow using the SSTs forecasts of the dynamical models and the proposed forecast algorithm.

529

530

531

532
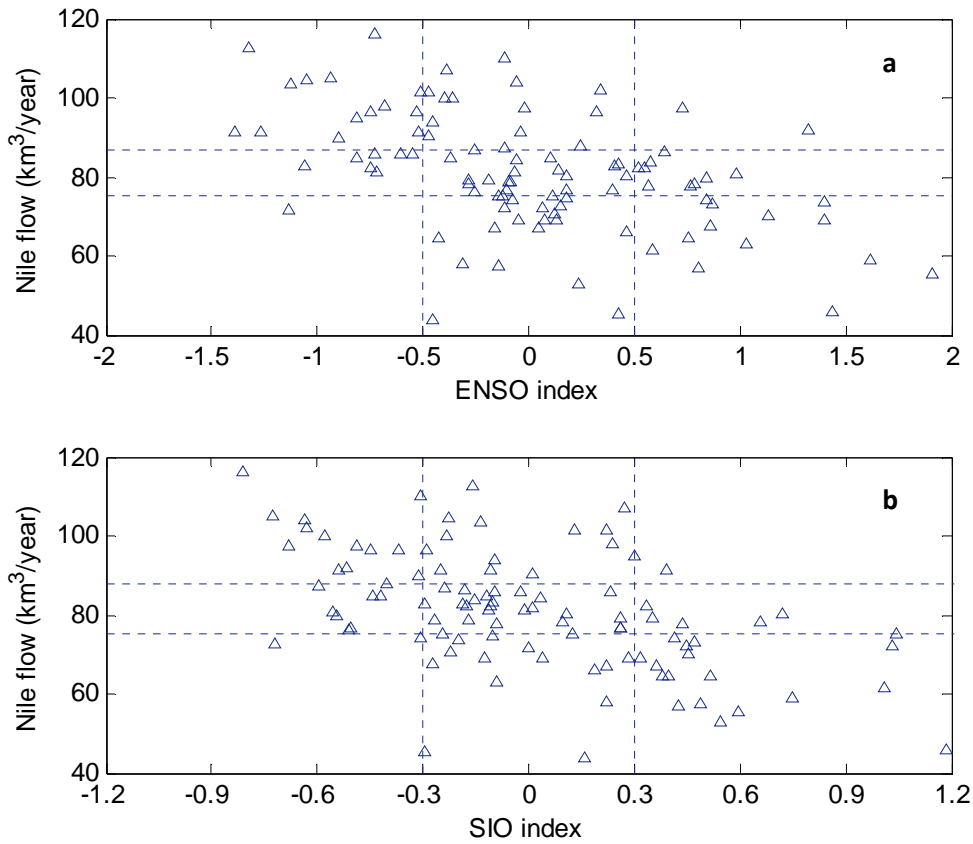
Figure 7: Relations between the annual Nile flow and different indices for the period (1900-2000): a) ENSO, and b) SIO. The horizontal lines represent the boundaries for the "high", "normal" and "low" categories of the annual flow. The vertical lines represent the boundaries for the "Warm", "normal", and "cold" conditions for ENSO and SIO indices.
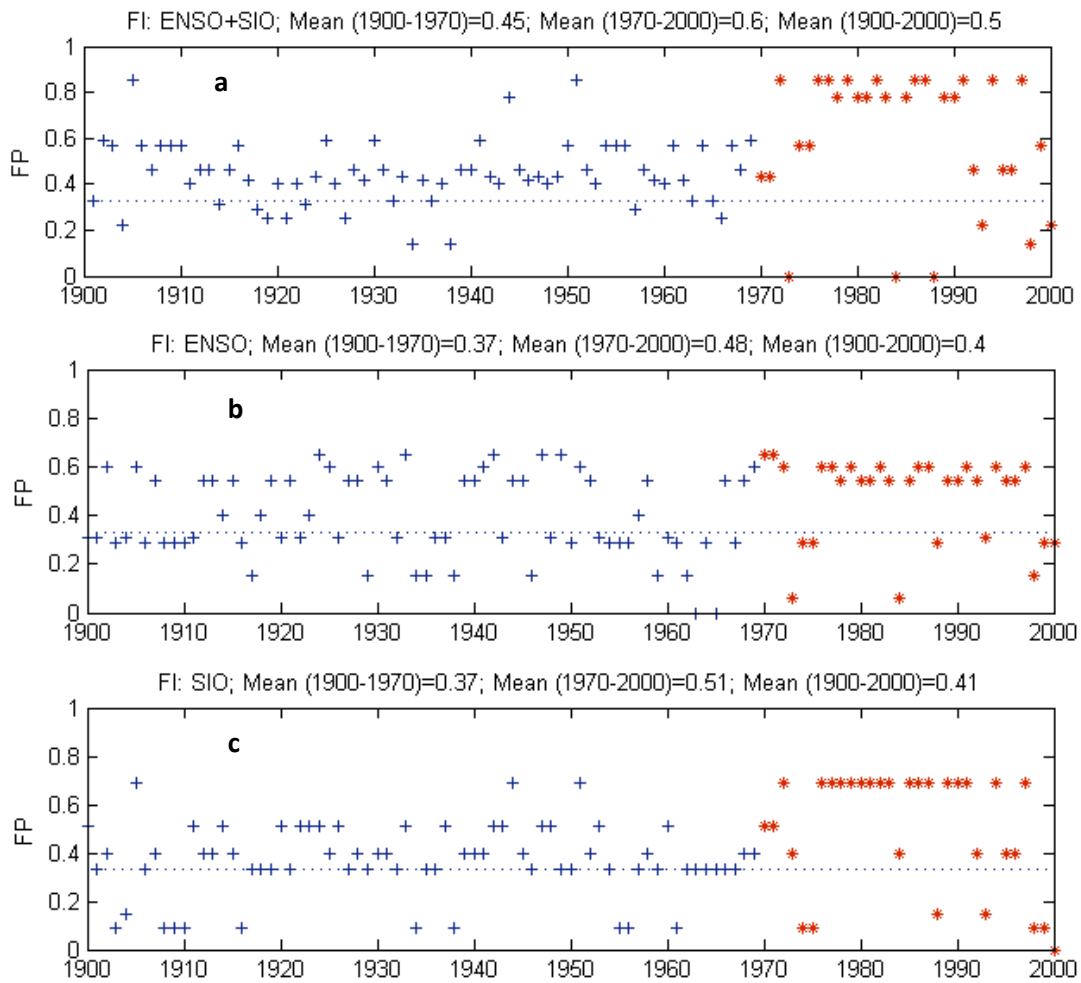
Figure 8: Time series of the forecast probability using different indices: a) ENSO and SIO together, b) ENSO, and c) SIO. The period (1900-1970) is used for calculating the probabilities (shown in crosses) using Eq. (2) and (1970-2000) for validation (shown in stars).